Galaxy Evolution across the Hubble Time
Proceedings IAU Symposium No. 235, 2006
F. Combes & J. Palouš, eds.

doi:10.1017/S1743921306010192

Massive and Evolved Galaxies at $z \geqslant 5$

T. Wiklind[1], B. Mobasher[1], M. Dickinson[2], H. Ferguson[3], M. Giavalisco[3], N. Grogin[4], and N. Panagia[3]

[1]ESA/STScI, Baltimore, MD 21218, USA
email: wiklind@stsci.edu

[2]NOAO, Tucson, AZ 85726, USA

[3]STScI, Baltimore, MD 21218, USA

[4]Johns Hopkins University, Baltimore, MD 21218, USA

Abstract. We search for massive and evolved galaxies at $z \geqslant 5$ in the Great Observatories Origins Deep Survey (GOODS) southern field. Combining HST ACS, VLT ISAAC and Spitzer IRAC broad–band photometric data, we develop a color selection technique to identify candidates for being evolved galaxies at high redshifts. The color selection is primarily based on locating the Balmer–break using the K- and 3.6 μm bands. Stellar population synthesis models are fitted to the SEDs of these galaxies to identify the final sample. We find 11 candidates with photometric redshifts in the range $4.9 < z < 5.6$, dominated by an old stellar population, with ages 0.2−1.0 Gyr, and stellar masses in the range $(0.7 - 5) \times 10^{11}$ $M_{\odot}$. Most of the candidates have modest amounts of internal dust extinction. The majority of the stars in these galaxies were formed at $z > 9$ and the current star formation activity is a few percent of the inferred initial star formation rate.

Keywords. galaxies: evolution, galaxies: formation, galaxies: high redshift

1. Introduction

An important goal of observational cosmology is to understand how stars are assembled into galaxies and how this is related to the evolution of dark matter halos. Finding the high-redshift galaxies and characterizing their stellar populations has always been a challenge. New observational techniques, in combination with new telescopes and instrumentation have now made it possible to start assessing the assembly of stellar mass in the early universe.

Identification of high-redshift galaxies using the the dropout technique has been a well-established procedure for almost a decade (Steidel *et al.* 1996). The contrast across the Lyman break, caused by absorption by intervening intergalactic matter, allows a clear distinction between foreground and high-redshift galaxies using broad band photometric observations. The dropout technique can be 'tuned' to select galaxies at different redshifts by selecting the appropriate filter combinations. Several thousands of Lyman-break galaxies (LBGs) have now been identified at redshifts from $z \approx 3$ to $z \approx 7$ (cf. Steidel *et al.* 1996; Bouwens & Illingworth 2006).

Alternative methods of selecting high redshift galaxies also relies on a contrast between different broad band filters. For instance, IRAC Extremely Red Objects (IEROs; Yan *et al.* 2004) are identified out to $z \approx 2$. 'BzK' objects at $z \approx 1.4$ (Daddi *et al.* 2004) and distant red galaxies (DRGs) at $z \approx 2$–3 (Franx *et al.* 2003). The latter are identified using the simple color criterion $(J-K) > 2.3$.

While the Lyman break technique preferentially selects UV-bright star forming galaxies, the alternative methods can be tailored to select more quiescent galaxies, i.e. those not actively forming stars. The methods are thus complementary if we are to make a

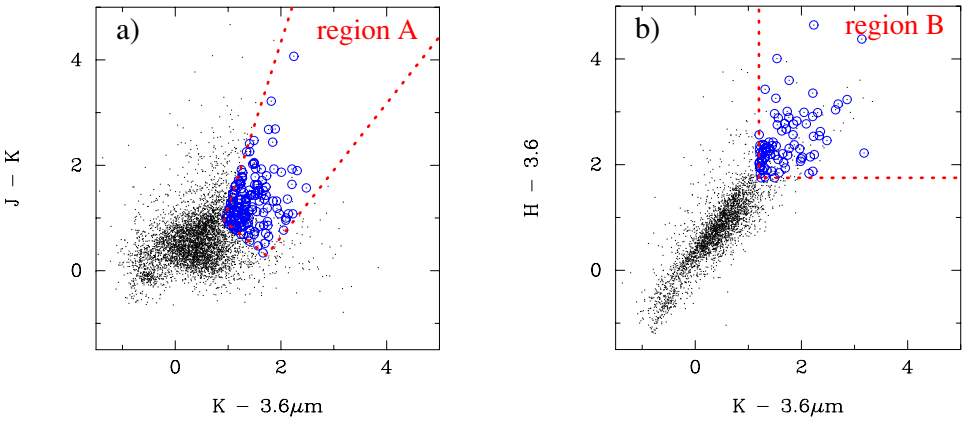

Figure 1. The color indices for the K_s-selected galaxies from the GOODS sample. Two alternative methods for selecting high redshift post-starburst galaxies using near- and mid-infrared colors. **a)** J−K vs. $K_s - 3.6\,\mu$m: the area inside the wedge outlined by the red line contains $z > 5$ post-starburst and dusty starburst galaxies. The selected candidates (shown as circles) will also contain dusty starburst systems at redshifts $z \approx 2$–8. **b)** H−3.6 μm vs. K−3.6 μm: the area above and to the right of the red line contains $z > 5$ post-starburst and dusty starburst galaxies.

complete inventory of the assembly of stellar mass at different redshifts. As the dropout technique is being extended to $z \approx 5$ and higher, we need a method to also search for passively evolving galaxies at the corresponding redshifts. It is only with the advent of satellites capable of observations in the near– and mid–infrared that it has become possible to pursue this goal.

2. Selecting evolved galaxies at $z \geqslant 5$

The 3648Å Balmer break is an age–dependent diagnostic of the stellar population. The break is most prominent in A–stars. In O– and B–stars, the hydrogen is mostly ionized, while in cooler late type stars, the opacity is dominated by H^-. For a single generation of stars, the break is most pronounced for ages between 0.1−1.0 Gyr. However, the development of the Balmer break occurs for stellar populations in both passively evolving and continuous star formation scenarios, but on different time scales (cf. Leitherer *et al.* 1999). The Balmer break has the potential to resolve the age–extinction degeneracy. Most extinction laws have a relatively smooth dependence on wavelength and will not produce the step-like feature of the Balmer break. Its usefulness, however, is limited by the photometric accuracy relative to the amplitude of the 3648Å break.

The sample used in this study is selected from the Great Observatories Origins Deep Survey (GOODS) southern field (Dickinson & Giavalisco 2003). This field has been observed at many wavelengths, including optical imaging (HST/ACS – BV*iz*; Giavalisco *et al.* 2004), near-infrared imaging (VLT/ISAAC – JHK_s; Vandame *et al.* in prep.), and deep mid–infrared imaging with the Spitzer Space Telescope with IRAC (3.6, 4.5, 5.7 and 8.0 μm; Dickinson *et al.* in prep.) as well as with the MIPS (24 μm; Charey *et al.* in prep.) instrument. The optical and mid–IR data sets cover the entire area of the GOODS-S ($16' \times 10'$). The near–IR images cover a slightly smaller area (137 arcmin^2). We construct a K–band selected catalog from the PSF–matched ACS (BV*iz*) and ISAAC (JHK_s) images, with total magnitudes. We coordinate–match the K–band detected sources with the Spitzer–IRAC catalogs for all the four channels, constructed separately for each channel,

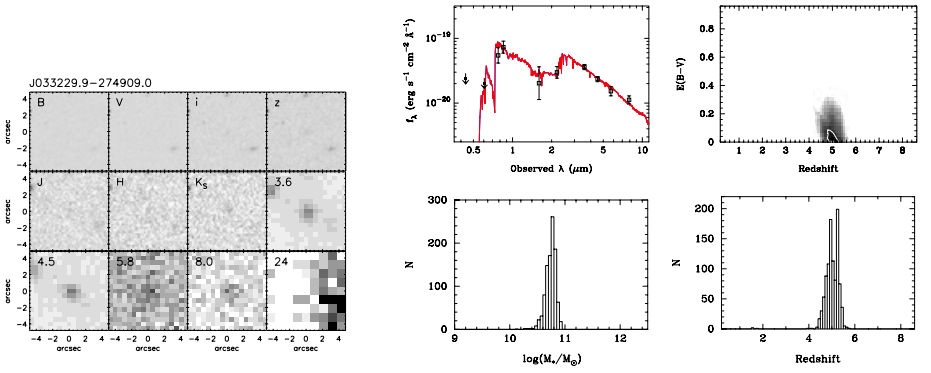

Figure 2. Results for one Balmer–break candidate in our sample. **Left:** Starting from the top left, the panels show the ACS BV*iz* bands, the ISAAC/VLT JHK$_s$ bands, the Spitzer IRAC 3.6, 4.5, 5.8, 8.0 μm bands and, finally, the Spitzer MIPS 24μm image. **Right:** *Top left:* The observed data with the best-fit model SED. *Top right:* Contours of χ^2_ν values for the best fit as a function of redshift and extinction E_{B-V}. Bottom panels show the results of 10^3 Monte Carlo realizations for redshift (right) and stellar mass (left) for the best fit solutions. The best-fit parameters for this Balmer break candidate are: $z = 5.0$; $E_{B-V} = 0.0$; age = 0.8 Gyr; $\tau = 0.2$ Gyr; $Z = 1.0\,Z_\odot$; $\log(M_*/M_\odot) = 10.75$.

using SExtractor and PSFs appropriate for that channel (Dickinson *et al.* 2006). In order to account for possible blending in the IRAC images, we performed manual PSF fitting on the IRAC images for the final sample of high-z candidates. Our final K$_s$ selected catalog contains 5754 sources and is ∼82% complete at $K_{AB} \approx 23.5$.

We use the stellar population synthesis models of Bruzual and Charlot (2003; BC03) to explore the broad–band color evolution of galaxies with different star formation histories, ages and metallicities. We use a Salpeter initial mass function, (IMF) with lower and upper mass cut-offs at 0.1 and 100 $M_\odot$, respectively. The resulting spectral energy distributions are redshifted in the range $z = 0.2$–8.6 with $\Delta z = 0.1$, and their colors are evaluated in the observed bands. Dust obscuration is parametrized using the attenuation law of Calzetti *et al.* (2000). Additional attenuation is introduced through neutral hydrogen absorption in the intergalactic medium (IGM). The age range considered extends from 5 Myr to 2.4 Gyr. Four different metallicities are used, 0.2, 0.4, 1.0, 2.5 $Z_\odot$. The star formation history is parametrized as an exponentially decreasing star formation rate, where τ represents the e–folding decay time.

An additional test of the confidence and stability of the model fitting can be obtained through Monte Carlo simulations, where the fluxes in all bands are allowed to vary simultaneously within their nominal errors. The errors are assumed to be normally distributed and uncorrelated. For our models, we generate 10^3 realizations of the photometric data set for each source. In each realization we retain the detections and upper-limits, but each photometric data point is allowed to vary stochastically as described above. We then determine the best–fit parameters for each realization of the photometric data. The distribution of redshift, age, stellar mass, extinction, etc. for the 10^3 Monte Carlo realizations represent probability distributions for the model parameters. This allows an estimate of the confidence level with better quality than a single realization and variation of the χ^2_ν values. The results for photometric redshift and stellar mass are used to determine the quality and the degree of confidence for the fitted parameters.

3. Results

Based on model tracks for post-starburst galaxies with ages >200 Myr, we define a region in K−3.6 μm vs. J−H, as well as in K−3.6 μm vs. H−3.6 μm color space (Fig 1). The reason for the two different color selection regimes is the slightly uneven coverage of J– and H–band data. In total the color selection selects ∼100 candidates in the two regions. The color selection includes a relatively large number of interlopers. By fitting synthetic spectral energy distributions to the broad-band data to the color selected candidates, we are able to extract a sample of 17 galaxies. These are further reduced by doing PSF fitting of the IRAC photometry, showing that in a few cases the IRAC fluxes are enhanced due to blending with neighboring sources.

The final sample of $z \geqslant 5$ and older than 200 Myr galaxies comprises 11 objects. The average redshift is $\bar{z} = 5.2$ and the average stellar mass is 2×10^{11} M$_\odot$. In general, the candidate galaxies contain no or only small amounts of dust. We model the star formation as exponentially decreasing, with a characteristic e–folding time scale τ. The allowed range for τ is 0−1 Gyr, i.e. instantaneous star burst to an approximately constant star formation rate. The star formation history of the Balmer–break candidates suggest that the major part of their stars were formed on a short time scale several Myrs earlier, putting the formation redshift in the range $z \approx 9 - 15$.

The effective comoving volume over which we sample the Balmer–break galaxies is $\sim 2.8 \times 10^5$ Mpc^3. This involves a completeness correction for the K–selection of 40%, but the total completeness, involving all aspects of the selection process, is difficult to estimate. The effective selection volume is therefore an upper limit. The stellar mass density, obtained by adding the masses of all 11 Balmer–break galaxies and the effective comoving volume, is 8×10^6 M$_\odot$ Mpc^{-3}. This represents 2–3% of the stellar mass density in the local universe and ∼20% of the stellar mass density found at $z \approx 2$. The number density of massive and evolved galaxies at $\bar{z} = 5.2$ is 4×10^{-5} Mpc^{-3}. Comparing with the expected number density of dark matter halos in concordant ΛCDM models, and using the Sheth–Tormen modification to the Press–Schechter formalism, this number density corresponds to a dark matter halo mass of 1×10^{12} M$_\odot$. This is lower than what is expected if the stellar–to–total mass ratio is the same as for the Milky Way galaxy and could indicate that the star formation efficiency is higher in the early universe than at $z \approx 0$.

References

Bouwens, R. J., & Illingworth, G. D 2006, *N*ature 443, 189
Bruzual, G., & Charlot, S. 2003, *M*NRAS 344, 1000
Calzetti, D., Armus, L., Bohlin, R. C., Kinney, A. L., Koornneed, J., & Storchi-Bergmann, T. 2000 *A*pJ 533, 682
Daddi, E., *et al.* 2004, *A*pJ 617, 746
Dickinson, M., Giavalisco, M., & the GOODS Team 2003, in: R. Bender & A. Renzini (eds) *T*he Mass of Galaxies at Low and High Redshift Springer Verlag
Franx, M., *et al.* 2003, *A*pJ 587, L79
Giavalisco, M., *et al.* 2004, *A*pJL 600, 93
Leitherer, C., *et al.* 1999, *A*pJS 123, 3
Maraston, C. 2005, *M*NRAS 362, 799
Steidel, C. C, Giavalisco, M., Pettini, M., Dickinson, M., & Adelberger K. L. 1996, *A*pJ 462, L17
Vanzella, E., Cristiani, S., Dickinson, M., Kuntschner, H., Nonino, M., Rettma, A., *et al.* 2006, *A*&A 454, 423
Yan, H., *et al.* 2004, *A*pJS 154, 75

Discussion

Ranga-Ram Chary: A note of caution : at z 1, dust-free red and dead galaxies like the LBDS ERO's have exactly the same SED as dusty starbursts like HR10, and can be discriminated only by 24 micron observations. Given the strong age-extinction degeneracy, your zero extinction fits are almost identical to dusty lower redshift fits.

Tommy Wiklind: Fits have been tested on other objects and appear to be robust.

Ranga-Ram Chary: Isn't it unusual that all objects with spectroscopic redshifts of z 6 have stellar masses which are 10^{10} $M_{\odot}$, but only the BBGs have $M_{star} > 10^{11}$ $M_{\odot}$?

Tommy Wiklind: Objects to be detected have to be massive, so there might be a selection effect.